AIAA 90-0510
Ultrasonic Measurement of the Geometric Parameters of Gaseous Voids in Low Gravity Fluid Containers

A. Patten and W. Durgin
Worchester Polytechnic Institute
Worchester, MA

28th Aerospace Sciences Meeting
January 8-11, 1990/Reno, Nevada

ULTRASONIC MEASUREMENT OF THE GEOMETRIC PARAMETERS OF GASEOUS VOIDS IN LOW GRAVITY FLUID CONTAINERS

A. T. Patten[1] and W. W. Durgin[2]
Worcester Polytechnic Institute
Worcester, MA

Abstract

A demonstration system for the ultrasonic gauging of fluids in low-gravity has been designed and tested. For purposes of simplification, it was assumed that vapor within a liquid container in low-gravity would form a spherical bubble which would float freely in the container. The project was designed to show that ultrasonic techniques could be used to determine the geometry of the resulting sphere given a worst-case transducer arrangement. The motivation was to simplify transducer mounting requirements so that propellant or other storage vessels could be fitted with ultrasonic gaging systems with a single or perhaps a few transducer penetrations. Data was collected from a planar array of transducers. The high error expected due to the low triangulation was reduced by maximizing the amount of data collected. This was accomplished using the transducers in both pulse/echo and pitch/catch operational modes.

Introduction

A long standing measurement problem in fluid mechanics has been the determination of liquid volume in low gravity wherein the liquid/vapor interface does not always occur at a consistent, locatable position. It has been proposed that ultrasonic imaging be used to establish the location and shape of a liquid/vapor interface in a liquid container, thus enabling liquid volume measurement [1,2].

Typically, in propellant storage applications, the liquid wets container walls so that a vapor bubble (or bubbles) exists within the liquid [3]. The liquid/vapor interface acts as a nearly perfect reflector of sound waves, so that it is then possible to project ultrasonic waves into the liquid, measure the reflected field using a transducer array, and compute the interface shape (and volume) from these data.

A limitation of conventional ultrasonic imaging schemes is that they require that the discontinuity reflect energy diffusely; that is, energy is reflected in all directions. Because the liquid/vapor interface approximates a perfect reflector, however, energy is reflected in primarily one direction. Conventional ultrasonic imaging schemes, such as those used in medical fields in addition to requiring diffuse reflection, require a mobile transducer or several transducer arrays. The added complexity of such a system would be objectionable especially with regard to cryogenic storage vessels. Transducers mounted on all sides of a container would provide a high degree of triangulation and therefore the high accuracy. The utility of such a system would be limited since access

[1]Student Member, AIAA.

[2]Member, AIAA.

to all sides of a vessel may be difficult or undesirable.

Ideally, it would be desirable to be able to "view" the entire fluid space using a limited planar array, idealized in Figure 1. Transmitted sound, reflected from fluid-vapor interfaces, would be received by other transducers whose signals would be analyzed to yield interface shapes and locations.

It seems that there are three basic requirements for ultrasonic imaging of a fluid/vapor interface. The first is that a technique must properly utilize the reflective properties of the interface. The second is that a small number of fixed transducers ought to be used. The third is that the transducers should be mounted in close proximity to each other, i.e. a single array.

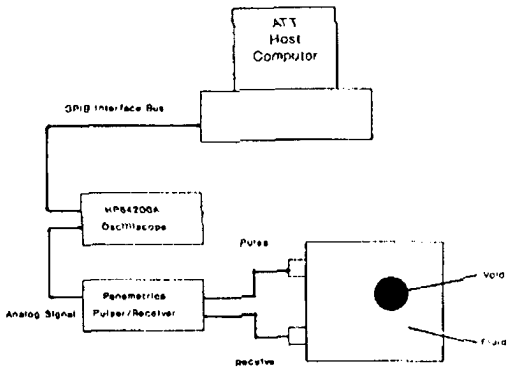

Figure 1 - Schematic of Test Setup. Pitch/Catch Mode Shown.

The objective of the work reported here was to show the feasibility of using ultrasonics with specific geometry constraints; namely, the transducers were mounted in a planar array, Figures 2 and 3. To this end it was assumed that bubbles tend toward the minimum energy state, ie. a single large bubble [4,5], and are free floating in the container [5]. Finally the assumption of sphericity implies that the bubble oscillations are damped [5,6].

Experimental Setup

The experiment was configured as in Figure 1. The pulser/receiver sent a negative 270 Volt square wave pulse to the transmitting transducer. The reflected pulse was then acquired by the receiving transducer, amplified by the receiver, and digitized. The digitized waveform was transmitted via the GPIB interface to the computer for analysis.

The pulser/receiver was used in two modes, the pitch/catch mode in which two transducers were used, and the pulse/echo mode where a transducer received its own signal. A synchronization port on the pulser/receiver was used to synchronized the electrical excitation pulse with the trigger on the oscilloscope.

Lens Design

Acoustic lenses are required for an application of this type to adequately spread the sound energy to all locations of the container as well as to receive sound from any location. As the wave number, k (Eq. 1) increases, the energy from the transducer becomes concentrated in a narrow beam centered on the axis of the transducer [8]. Since it is desired to be able to detect an object anywhere in the container a lens was necessary to spread the energy from the transducer axis more or less equally in all directions. Hemispherical polystyrene lenses were constructed and mounted on the transducers to achieve such de-focusing. The signal strength with the lens attached was strong enough to detect the ultrasonic pulses up to 25° of the transducer axis. Beyond 25° the signal to noise ratio was too low to detect the signal because polystyrene is highly absorbative to sound in the high frequency range.

$$k = 2\pi f/c \qquad \text{(Eq. 1)}$$

where f = Transducer center frequency
c = Sound speed

Transducer Arrangement and Beam Overlap

Five transducers were used throughout the experiment. Figure 2 shows the end view of the container with the

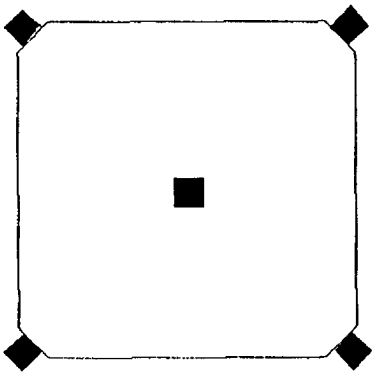

Figure 2 - End View of Container.

mounted transducers. Figure 3 shows the side view of the container. The mappable region is axisymmetric about the center transducer.

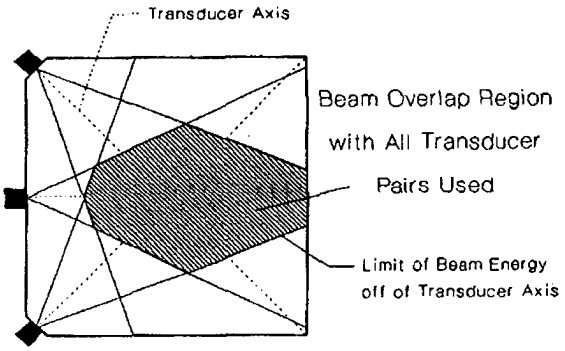

Figure 3 - Transducer Configuration Maximizing Beam Overlap.

Simulated Gas Bubbles

Glass and steel spheres were used to simulate low gravity bubbles. Since the density and sound speed of glass differ significantly from water, an acoustic impedance mismatch exists and a reflection results. The same phenomenon occurs at the interface between a fluid and gas. Impedance is given by Equation 2 [8].

$$Z = pc \qquad \text{(Eq. 2)}$$

where p = Density
c = Sound speed in medium

Measurements and Results

A primary goal of this project was to allow the mapping of a container with stationary transducers mounted in close proximity to each other. In this experiment the transducers were mounted on essentially the same plane. It has been shown [2] that when transducers are mounted such that the triangulation is high an acceptable level accuracy may be obtained, Figure 4. However, with transducers mounted on the same plane triangulation is lost in one direction.

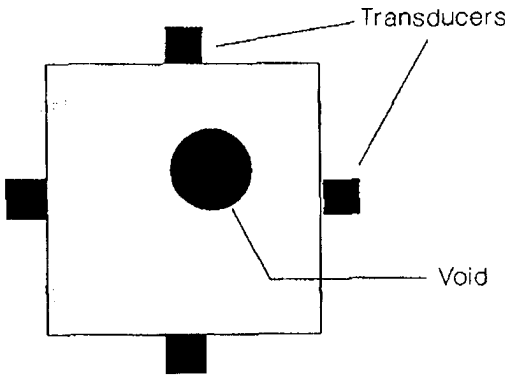

Figure 4 - Transducers Mounted for Maximum Triangulation.

If the transducers are mounted as in Figure 4, the only signals which can be obtained are the ones defined when a transducer receives its own signal (the angle from the transducer axis is otherwise too great for the available lenses and the signal to noise ratio is small). A benefit, then, of a planar array is that the transducers may be allowed to communicate and increase the amount of data collected. For a system of five transducers, fifteen unique data points are

defined along with fifteen geometric equations. The equations constitute an overdefined system that can be solved simultaneously for the unknown void parameters. An algorithm to determine the least square fit of these data was developed and implemented.

Algorithm Description

A propagating wave front must specularly reflect from a bubble surface and the reflection must be so that the angle of incidence is equal to the angle of reflection. Since the bubble is spherical, the center of the sphere must lie 1) on the same line as the transducer location if it receives its own signal or 2) on the plane made by the center and the two transducers in a pitch/catch mode.

If a transducer receives its own signal, then it must be that the reflection came from the point on the sphere where the sphere normal points at the transducer. It follows that the sphere center, the transducer, and point of incidence all lie on the same line. The

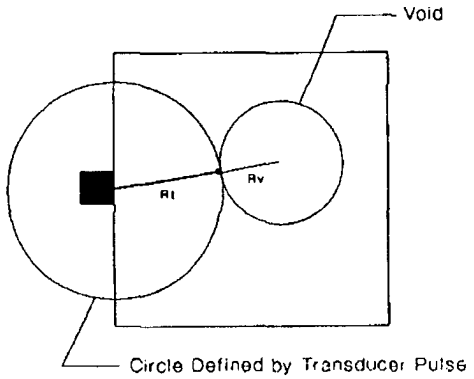

Figure 5 - Single Transducer Sends and Receives a Signal.

problem reduces to a one dimensional one with the equation of a circle defined by the transducer location and the propagation time, Figure 5. The void radius then is the distance from the center of the sphere to the transducer minus the radius of the circle defined by the transducer pulse [2]. Mathematically this is given by Equation 3.

$$r_v = r_c - r_t \qquad \text{(Eq. 3)}$$

where r_v = Sphere radius

r_c = Distance from the sphere center to the transducer

r_t = Circle defined by pulse time

For the case of two transducers where one transmits and the second receives, the point of reflection and the two transducers must lie on the same plane. In this case, the sphere normal lies in the plane defined by the three points so the sphere center also must lie on

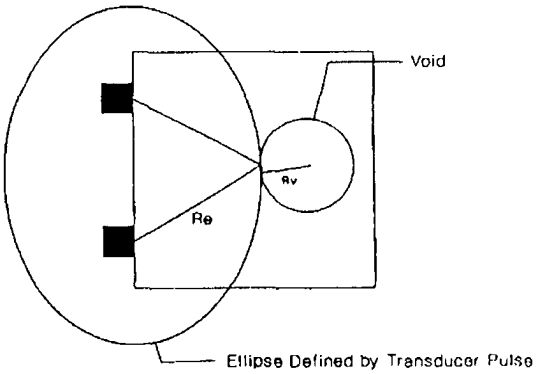

Figure 6 - Pitch/Catch Operation Mode.

the plane. This problem reduces to a two dimensional one with an ellipse defined by the two transducers (the foci) and the propagation time (ellipse radius), Figure 6. The void radius is the minimum distance from the center of the sphere to the equation defined by transducers. The computer algorithm rotates the coordinate system such that the origin is between the foci. An iterative routine finds the minimum distance from the center to the ellipse equation. An initial guess of the tangency point (X_p,Y_p) between the ellipse and the unknown sphere was taken as the point on the ellipse that intersected the line connecting the sphere center and the coordinate axis origin. The point (X_p,Y_p) was corrected based on the slope at (X_p,Y_p) until the minimum distance to the sphere center was

found. Figure 7 shows an example of the iteration to arrive at the sphere radius for a given center location.

Sphere Center (X,Y) = (10.2991,3.4862)
Initial Ellipse Intersection (Xp,Yp) = (5.5356,1.8738)
Initial Sphere Radius = 5.0289

Ellipse Slope at (X_p,Y_p)	Normal at (X_p,Y_p)	New Y_p = $Y+(X-X_p)$*Normal	X_p-	Sphere Radius
4.52	-0.22	2.43	5.39	5.0193
3.39	-0.29	2.04	5.50	5.0152
4.12	-0.24	2.32	5.42	5.0128
3.57	-0.28	2.12	5.48	5.0117

Figure 7 - Sample Calculation Showing Iteration to Find Sphere Radius in Pitch/Catch Mode. Dimensions in Inches.

The Best Fit Sphere

The description above has assumed that the sphere center is known. A usable algorithm must find the center as well as the radius. The approach taken was to solve the inverse problem; that is, assume a center and calculate a radius. The container was broken into a mesh of grid points and the radius calculated at each grid point. The average radius and the standard deviation were then found. The grid point at which the standard deviation was a minimum was taken to be the center. The mesh was refined with a recursive algorithm until the standard deviation became constant within 0.01%. This error level resulted in a typical recursion level of five or six.

Data could not be collected from all fifteen transducer combinations at all times. The signal to noise ratio was too small to identify the signal of every transducer pair when the void was at tank extremes.

Error Analysis

The algorithm was verified using actual test data and by the introduction of errors to "exact" artificial data. As expected, the lack of triangulation proved to be a major problem. It was difficult to predict accurately the center location in the direction away from the transducers with concomitant degradation in void radius occurring. The problem was ultimately overcome by the large amount of data that was collected.

It was originally thought that very high frequency sound should be used to minimize the wavelength and increase the resolution. For this reason, 15 MHz transducers were used. Due to the disproportionate attenuation of high frequencies and the addition of the polystyrene lens, the effective transducer frequency was 2 MHz. As a result, the wavelength and thus system resolution was approximately 0.03". Since good results were obtained, this lower resolution of the ultrasound proved to be less important that the amount of data collected. In addition, the rather imprecise machining tolerance of ± 0.01" was of little consequence.

Expected Error

The error in calculating the void radius is largely dependent on three parameters:

1) The propagation time error,

2) the number of data points collected, and

3) the transducer locations and hence the amount of triangulation.

To quantify the error, the computer program described above was used "in reverse". That is, a radius and center location were specified and the pulse times required to satisfy these data were calculated. These data then represented the exact solution. To approximate the actual system, errors expected in the actual experiment were introduced to this exact data.

Typical errors associated with ultrasonic measurements are taken to be one wavelength of the propagating sound. Therefore, one wavelength of the effective transducer frequency of 2 MHz was used as the maximum error associated with each pulse; error was added to each pulse based on a normal distribution.

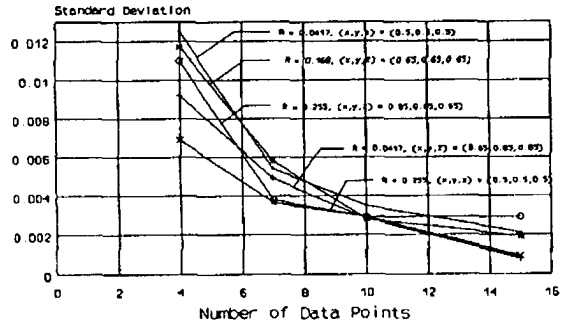

Figure 8 - Expected Void Radius Error vs. Number of Data Points. Error Based on 1 Wavelength Resolution (2 MHz).

Figure 8 shows the standard deviation of the void radius. To generate this plot ten samples were taken for each data point and the standard deviation calculated. Three sphere radii were used at two container locations. From this plot it can be seen that the error is approximately constant with respect to radius and tank location. This is reasonable since the propagation time is the same order of magnitude regardless of radius and location, and one wavelength is small relative to the total path length.

If the geometry is specified and constant, the error is a function only of the number of data points collected. Figure 9 shows the expected error as a function of the number of data points collected for the three radii used in the experiment. The expected error is based on the maximum standard deviation of Figure 8.
Since the error is constant with respect to the radius, the relative amount that the radius is in error increases as the radius decreases. This is not a serious consequence since small bubbles are a small percentage of the total volume.

Figure 10 shows a plot of expected error vs. frequency. The graph was generated in the same way Figure 7 was derived. Based on these data, it is advisable to maintain a minimum frequency of approximately 1 MHz.

Experimental Results

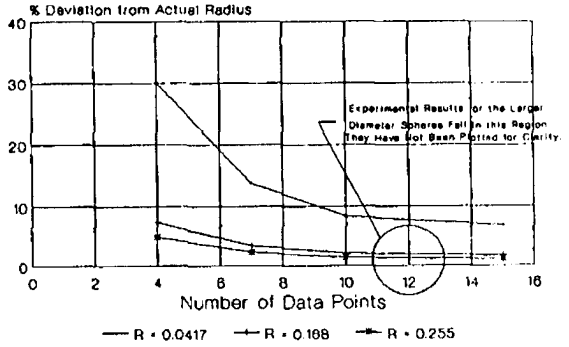

Figure 9 - Maximum Expected Radius Error.

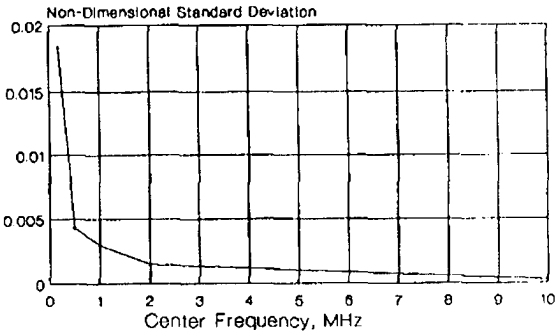

Figure 10 - Expected Error vs. Frequency. R=0.255, (x,y,z)=(0.5,0.5,0.5), Number of Points = 15.

Table 1 shows the results of the experiment. The data for the two larger radii check closely with the analytic results of Figure 9 with 12 data points. Only six points were usable when the smallest sphere was located away from the center of the container (predicted radius = 0.065). The six data points collected are of questionable accuracy as well, due to the low signal strength resulting from the small amount of energy reflected from a large curvature (small radius) object. The detection of small objects is therefore difficult, in general. The data for the small sphere located in the center of the container was taken with no lenses and hence a high signal to noise ratio. This was possible because the angles off the transducer axes were small.

Sphere Radius	(x,y,z) Location	Predicted Radius	Percent Error with Respect to		Number of Points Collected	Lens Used?
			Radius	Volume		
0.0417	0.48,0.50,0.88	0.040	-4.6	-11.	16	No
	0.72,0.44,0.89	0.008	80.	280	0	Yes
0.100	0.77,0.76,0.46	0.172	2.0	0.1	12	Yes
	0.80,0.48,0.46	0.171	1.0	4.0	12	Yes
0.286	0.88,0.48,0.87	0.288	1.3	4.2	12	Yes
	0.76,0.76,0.60	0.280	-2.0	-6.0	12	Yes

Table 1 - Experimental Results.
All Dimensions are Non-Dimensional with Tank Length.

Conclusions

The results show that it is possible to utilize ultrasonic imaging techniques based on specular reflection to determine the location and radii of spherical interfaces. Furthermore, this can be accomplished with a planar transducer array.

There are, to be sure, many shortcomings and limitations which must be overcome prior to implementation of such a technique for liquid gaging. It is clear that better lens materials must be found to minimize attenuation and broaden the field of view. It is also clear that much greater data acquisition speed will be required when real interfaces which will oscillate must be imaged. In principle, nevertheless, such gaging techniques will work.

Additionally, storage vessels will utilize various liquid control and acquisition devices. It is likely that such devices can be utilized to maintain the liquid vapor interface within the field of view of the array. With adequate redundancy and suitable signal to noise ratio, near spherical interfaces can be measured with such a system.

References

1. Jacobson, Saul A., et al, Low Gravity Sensing of Liquid/Vapor Interface and Transient Liquid Flow, *IEEE Transactions on Ultrasonics, Ferroelectrics, and Frequency Control, Vol. UFFC-34 No. 2*, March, 1987.

2. Roberti, Dino, An Investigation Using Ultrasonic Techniques to Determine Parameters of Voids, Master's Thesis, WPI, 1987.

3. Concus, P., On Existence Criteria for Fluid Interfaces in the Absence of Gravity, *Waves on Fluid Interfaces*, (ed. Meyer, Richard E.), Academic Press, 1983.

4. Reynolds, William C., Satterlee, Hugh M., Liquid Propellant Behavior at Low and Zero G, Chapter 11 of NASA SP-106 *Dynamic Behavior of Liquids*, (ed. Abramson, H. N.), 1966.

5. NASA Film on Low Gravity Fluid Behavior, NASA (in possession of Prof. W. W. Durgin at WPI),

1987.

6. Lamb, Horace, *Hydrodynamics*, Dover, 1945.

7. Wang, T. G., Saffren M. M., Elleman, D.D., Drop Dynamics in Space, Jet Propulsion Laboratory at California Inst. of Technology, ESA Special Publication No. 114, 1977.

8. Kinsler, Lawrence E., *Fundamentals of Acoustics*, Wiley, 1982.